Physics of the Solid State, Vol. 45, No. 6, 2003, pp. 1177–1184. Translated from Fizika Tverdogo Tela, Vol. 45, No. 6, 2003, pp. 1122–1129.

LOW-DIMENSIONAL SYSTEMS AND SURFACE PHYSICS

Structure and Physical-Mechanical Properties of Nanostructured Thin Films

D. V. Shtanskiĭ*, S. A. Kulinich, E. A. Levashov*, and J. J. Moore*****

** Moscow Institute of Steel and Alloys, Leninskiĭ pr. 4, Moscow, 119991 Russia*

e-mail: shtansky@shs.misis.ru

*** National Institute for Materials Science, Sakura 3-13, Tsukuba, 305-0003 Japan*

**** Colorado School of Mines, Golden, Colorado, 80401-1887 USA*

Received October 8, 2002; in final form, November 19, 2002

Abstract—The structure and mechanical properties of nanostructured thin films based on carbides, nitrides, and borides of transition metals are described. The mechanisms of localized deformation of the films during indentation are compared. It is shown that the tendency of a material to form shear bands during deformation can be predicted using the parameter H^3/E^2, which describes the resistance of the material to plastic deformation. The columnar structure of the films is found to play an important role during deformation, which proceeds via slipping of columnar structural elements along the direction of an applied load. © *2003 MAIK "Nauka/Interperiodica".*

1. INTRODUCTION

The structures of nanomaterials differ from those of ordinary materials, which thus leads to the discovery of new physical phenomena as a result of the unique structure and properties of nanomaterials. Surface engineering has currently reached the nanometer scale. However, significant problems were encountered regarding both fundamental understanding of the behavior of nanosystems and quantitative measurements and interpretation of their properties, and this has hampered the development and application of nanotechnologies [1, 2].

Tribological coatings should have low abrasive wear, high fatigue strength, and high resistance to deformation and fracture. According to the classical theory of wear, low abrasive wear is ordinarily related to high hardness (which has been repeatedly borne out for films [3, 4]) and high fatigue strength corresponds to high values of the Young's modulus. In real practice, the hardness H of a material is usually measured; however, this quantity is a dependent characteristic and is connected with the elastic and plastic properties of the material. The hardness of nanostructured films can be as high as 50–70 GPa [3] and even exceed that of polycrystalline diamond [5]. Most bulk materials with high hardness exhibit high values of the modulus of elasticity E, which makes them brittle. To estimate the resistance of materials to elastic strain to failure, the ratio of the hardness to the elastic modulus H/E, which is also called the plasticity index, is used. To estimate the resistance of materials to plastic strain, the parameter H^3/E^2 is applied [6]. Whence it follows that, in order to possess an increased resistance to elastic breaking strain and a decreased plastic strain, a material should have high hardness and a low modulus of elasticity. One of the methods for producing materials with a high H/E ratio is the deposition of nanostructured coatings.

An interesting feature of hard, superhard ($H \geq 40$ GPa), and ultrahard ($H \geq 70$ GPa) nanostructured films is that, apart from high hardness, they also have high strength and elastic recovery W_e (up to 90%) [7, 8]. Thus, we deal with a new class of materials that have high hardness and elasticity and allow intentional variation of the values of H, E, and W_e. The elastic behavior of nanostructured films can be caused by an absence of internal sources of dislocations in nanocrystals of sizes below a certain critical value [9]. In this case, the mechanism limiting the deformation of nanostructured films is diffusion mass transfer and/or grain-boundary slip, whereas dislocation motion is hindered because of small crystallite size and the presence of intergrain amorphous layers. The strength of the interface, whose volume fraction can be as high as 50%, becomes one of the key factors determining the deformation of nanomaterials. Moreover, the critical crack size in nanomaterials coincides with the size of crystallites and is only a few nanometers. Therefore, it was assumed that nanostructured materials cannot deform plastically. Vepřek and Reiprich [10] believe that multiple nanocracks, which cannot grow above a critical size specified by crystallite size, appear during deformation of nanostructured films. Upon unloading, these nanocracks become closed, thus leading to the partial or complete recovery of deformed regions. This hypothesis is in conflict with a number of experimental results. For example, the authors of [9, 11–13] showed that the deformation of nanostructured films can be both homogeneous and inhomogeneous (localized, with the formation of shear bands). Plastic deformation in localized

Table 1. Basic deposition parameters and film structures

Film composition	Deposition parameters			Film structure		
	temperature, °C	bias voltage *V*, V	nitrogen partial pressure (N_2/Ar)	crystal structure	grain size, nm	film morphology
Ti–B–N (1)	250	–250	0	NaCl	10–40	Equiaxed grains
Ti–B–N (2)	400	0	0	NaCl	4–10	"
Ti–Cr–B–N	250	0	0.15	NaCl	2–7	"
Ti–Si–N	250	0	0.15	NaCl	10–30	Columnar grains
Cr–B	250	–250	0	AlB_2	1000*	"

* Each columnar grain consists of grains and subgrains 20-–40 nm in size.

Table 2. Mechanical properties and roughness of films

Film composition	Hardness *H*, GPa (Si substrate)	Elastic modulus *E*, GPa	*H*/*E*	H^3/E^2, GPa	R_{rms}, nm	Elastic recovery W_e, %
Ti–B–N (1)	34	250	0.136	0.63	1.15	81
Ti–B–N (2)	42	300	0.140	0.82	4.5	77
Ti–Cr–B–N	27	240	0.112	0.34	0.3	73
Ti–Si–N	24	210	0.114	0.31	1.3	76
Cr–B	33	276	0.119	0.47	1.0	73

regions is typical for amorphous materials and was also observed in some nanostructured and ceramic materials. Although there are various models for the deformation of materials via the formation of shear bands [14], this phenomenon has not been properly explained.

The microstructure of single-phase films is usually well described by the model of structural zones [15, 16]. According to this model, films prepared under the conditions of low mobility of adsorbed atoms have a strongly anisotropic columnar structure. This structure often appears in films grown through physical deposition and causes undesirable stresses parallel to the surface of the substrate. Localized strain in films with a pronounced columnar structure is assumed to develop homogeneously, whereas the formation of shear bands is typical of films with an equiaxed-grain structure [9, 11–13].

The purpose of this work is to describe the behavior of nanostructured films based on carbides, nitrides, and borides of transition metals under localized deformation and to reveal an interrelation between their structure and physical-mechanical properties.

Composite targets to be sputtered were fabricated through the process of force SHS compacting (self-propagating high temperature synthesis) from exothermic blends of different powders [17]. Thin films were deposited through magnetron sputtering of the composite targets in an argon atmosphere or a gaseous mixture of argon and nitrogen. The temperature and bias voltage were varied (Table 1). For substrates, we used (001) silicon single crystals, nickel, stainless steel, and a VK-type hard alloy. The structure of coatings was studied using a Hitachi S-4200 scanning and a Hitachi-9000NAR transmission electron microscope. Foils for a high-resolution electron microscopic study of transverse sections were prepared following the standard technique [1]. A Geigerflex diffractometer was used for x-ray diffraction analysis. Depth profile analysis of the film composition was performed using Auger electron spectroscopy on an LHS-10 SAM apparatus. The hardness, modulus of elasticity, and elastic recovery were measured on a TriboScope device (Hysitron, Inc., USA) and a nanohardness tester (CSM Instruments, Switzerland) by following the Oliver and Pharr technique [18]. Localized deformation in films was initiated with a tetrahedral Vickers pyramid under loads of 10, 25, and 50 g. Film surface topography before and after indentation was studied using NanoScope III (Digital Instruments, US) and NanoScan (Russia) atomic-force microscopes (AFMs).

2. FILM STRUCTURES

Table 2 gives the root-mean-square values of the surface roughness R_{rms} of films measured using AFM with an accuracy of 5%. The film roughness is seen to depend on both the chemical composition and parameters of the physical deposition. The smoothest surface was detected in the Ti–Cr–B–N films, which inherited the roughness (0.2 nm) of the silicon substrate after ion etching. When a bias voltage is applied, the outer layers of a film are sputtered by ions of a working gas and then deposited, which smoothens the film surface. However,

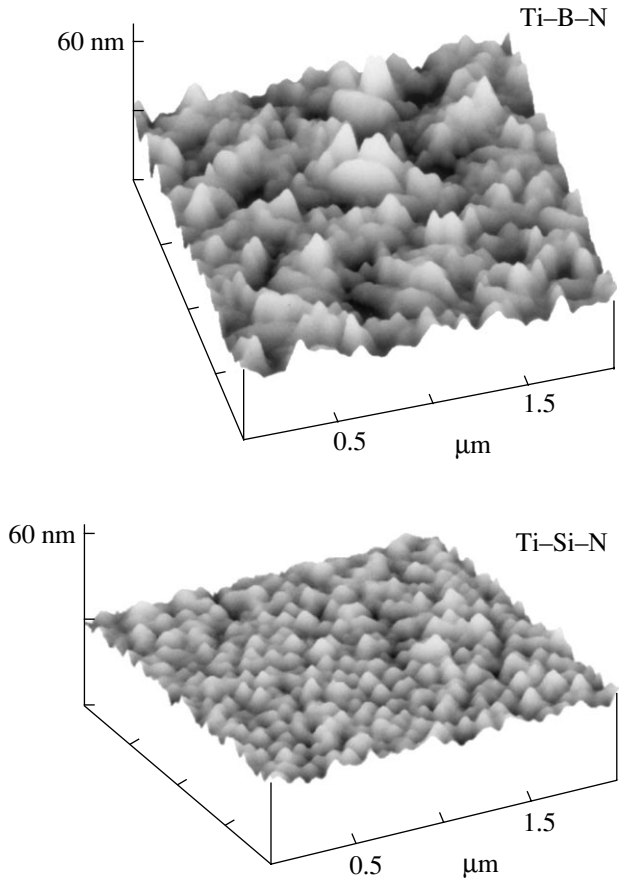

Fig. 1. Surface topography of Ti–B–N (2) and Ti–Si–N films.

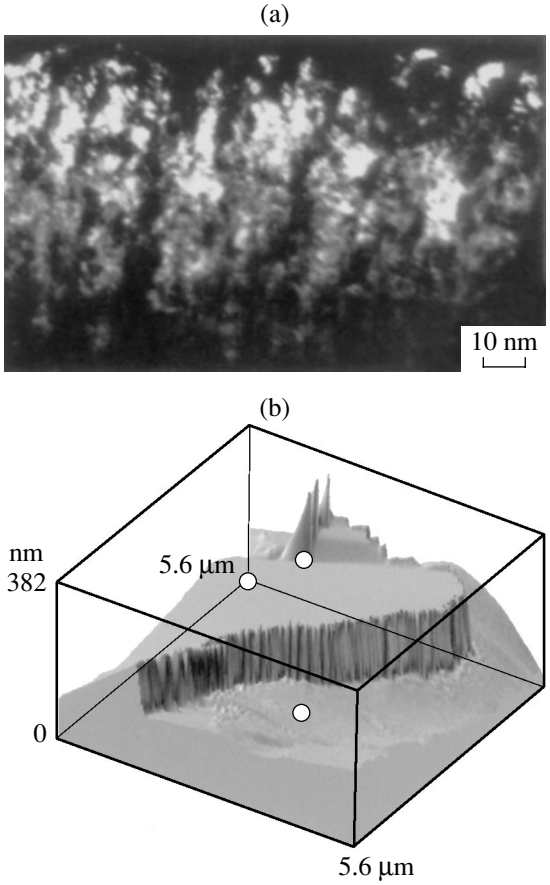

Fig. 2. Films with a columnar structure: (a) electron microscopic dark-field image of the cross section of a Ti–Si–N film and (b) fractograph of the fracture surface of a CrB_2 film.

in the case of multicomponent films, a perfect surface can be prepared without applying a bias voltage. With increasing substrate temperature, the film surface roughness increases because of the increased mobility of deposited atoms and their diffusion to islands formed earlier. AFM images (Fig. 1) show that the film surfaces are covered with three-dimensional hillocks 40–50 nm (Ti–Cr–B–N), 60–70 nm (Ti–Si–N), 80–100 nm (Ti–B–N (1)), 130–140 nm (CrB_2), and 170–190 nm (Ti–B–N (2)) in size. The nature of these hillocks is usually connected with the film growth mechanism, i.e., with the formation of separate islands on the substrate surface (the Volmer–Weber mechanism) and their growth and coalescence, which result in the formation of intergrain cavities due to the shielding effect.

The results of the structural analysis are given in Table 1. The structures and morphology of the films are seen to differ significantly. The Cr–B and Ti–Si–N films have a pronounced columnar structure with columns 10–30 nm and 0.1 μm in diameter, respectively (Fig. 2). Columnar grains in the latter films, however, contain many equiaxed grains and subgrains, which means that the actual size of crystallites in them (20–40 nm) turns out to be substantially smaller than the width of columnar macrograins. Note that a columnar structure with many crystallites inside its elements was observed earlier in [19]. The cross-sectional electron microscopic study of the Ti–B–N and Ti–Cr–B–N films showed the absence of a columnar structure (Figs. 3a, 3b). A dark-field image of the structure of the Ti–Cr–B–N film demonstrates crystallites 2–7 nm in size (Fig. 3c). The corresponding electron diffraction pattern shows that they have a cubic NaCl-type structure. Note that the film grows along the image plane, which indicates the absence of a columnar structure. Instead, TiN-based equiaxed grains and intergrain amorphous regions are formed. Figure 3d shows a high-resolution micrograph of a Ti–Cr–B–N film with a separate TiN nanocrystallite 3–4 nm in size oriented along the ⟨001⟩ zone axis.

It is interesting that Ti–Si–N and Ti–Cr–B–N films deposited under identical conditions ($T = 250°C$, $V = 0$, $N_2/Ar = 0.15$) have different morphology, namely, a columnar grain structure in the former case and an equiaxed-grain structure in the latter. The formation of a strongly anisotropic columnar structure is ordinarily

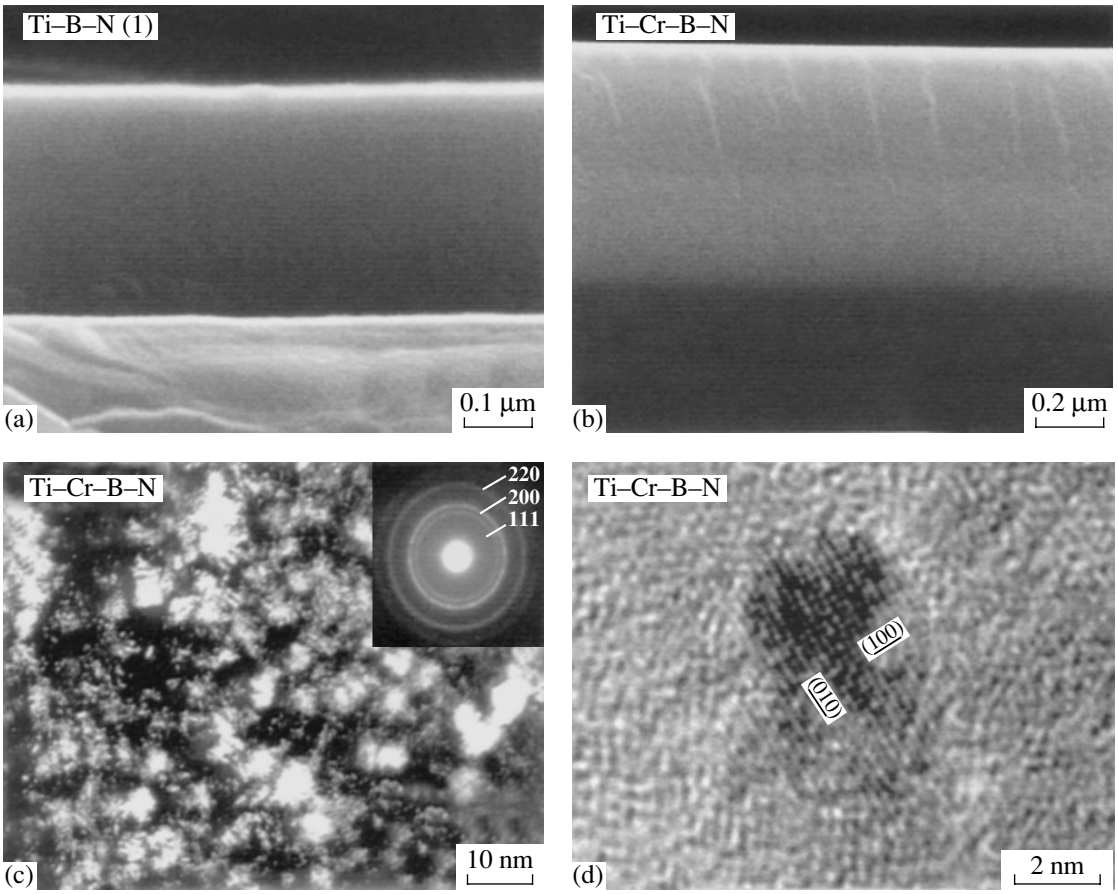

Fig. 3. Electron microscopic images of films with an equiaxed-grain structure: (a, b) scanning, (c) dark-field, and (d) high-resolution images.

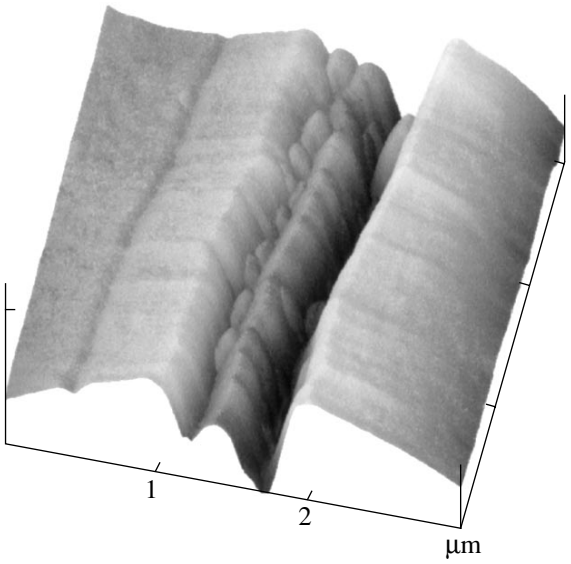

Fig. 4. Fractograph of the fracture surface of a Ti–Cr–B–N film after scratching its surface with a diamond pyramid.

related to segregation of impurities along grain boundaries when the mobility of adsorbed atoms is low [15, 16]. Our results indicate that the structure of a multicomponent film cannot be unambiguously predicted using the model of structural zones, which performed

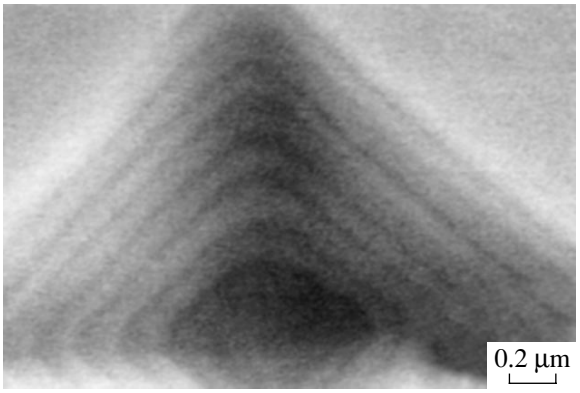

Fig. 5. Electron microscopic image of an indentation made by a Vickers pyramid in a Ti–Cr–B–N film at a load of 25 g.

Table 3. Deformation types of nanostructured thin films (published data)

Composition	Crystal structure	Morphology	References
Homogeneous deformation			
TiN	NaCl	Columnar	[9]
(Ti, Al)N	NaCl	"	[11–13]
Ti(B, N)	AlB_2	"	[11–13]
Inhomogeneous deformation			
TiB_2	AlB_2	Partially columnar or lumplike	[9]
AlN	ZnS	"	[11–13]

well for single-phase films. For a multiphase system, it seems to be difficult even to establish the basic parameter T/T_m (T_m is the melting point), which specifies the surface mobility of deposited particles of a material. The introduction of additional elements into the composition of coatings can hinder the growth of a columnar structure and stimulate the nucleation of new grains, thus leading to an equiaxed-grain structure at various temperatures.

Three-dimensional islands on the surface of the films with a columnar structure are the places where the ends of individual grains come to the surface. The characteristic scale of the surface relief for the films with an equiaxed-grain structure (80–100 nm for Ti–B–N (1), 180 nm for Ti–B–N (2), and 40–50 nm for Ti–Cr–B–N) exceeds the size of crystallites in these films (10–40, 4–10, and 2–7 nm, respectively) by an order of magnitude. When films are deposited onto a surface, hollows and grooves form, decreasing the total surface energy [20]. These regions have a low density because of the high volume fraction of pores, defects, and incoherent interfaces. The formation of such interfaces results in a latent columnar structure. Although this structure cannot be revealed when cross-sectional fracture surfaces of films are examined with a scanning electron microscope, it plays a decisive role in deformation. Figure 4 shows a fracture micrograph for a Ti–Cr–B–N film after scratching its surface with a diamond indenter. A pronounced columnar structure is visible after deformation, and its geometry correlates with the film surface topography. It is seen that, in the process of deformation, individual columns or columnar structural elements (CSEs) consisting of many crystallites slip with respect to each other.

3. LOCALIZED DEFORMATION IN THIN FILMS

For fractography analysis, we chose films differing in crystal structure, grain size, and grain morphology (Table 1), according to data on the deformation types of nanostructured films obtained earlier (Table 3).

Figure 5 shows an electron microscopic image of an indentation made with a Vickers pyramid at a load of 25 g in a Ti–Cr–B–N film deposited onto a silicon substrate. The applied load is seen to cause shear bands

Table 4. Formation of shear bands and particles rejected outside (PROs) in regions of localized deformation

Film composition	10 g		25 g		50 g	
	shear bands	PROs	shear bands	PROs	shear bands	PROs
Ti–B–N (1)	–	+	–	+		
Ti–B–N (2)	–	–	–	–	–	–
Ti–Cr–B–N	+	+	+	+	+	+
Ti–Si–N	–	–	+	–	+	+
Cr–B	–	–	–	–	+	+

Table 5. Comparison of the values of hardness, elastic modulus, and elastic recovery obtained in this work for multicomponent films with published data

Film composition	Hardness H, GPa	Elastic modulus E, GPa	Elastic recovery W_e, %	H^3/E^2, GPa	References
Ti–Si–N	42.3	273	78	1.02	
Ti–Zr–C–O	41.9	289	77	0.88	
Ti–B–N	42.0	300	77	0.82	
Ti–Ca–C–O	41.4	325	68	0.67	
Ti–Al–N	41.9	397	74	0.46	[24]
Ti–Mo–N	43.0	442	68	0.41	[25]

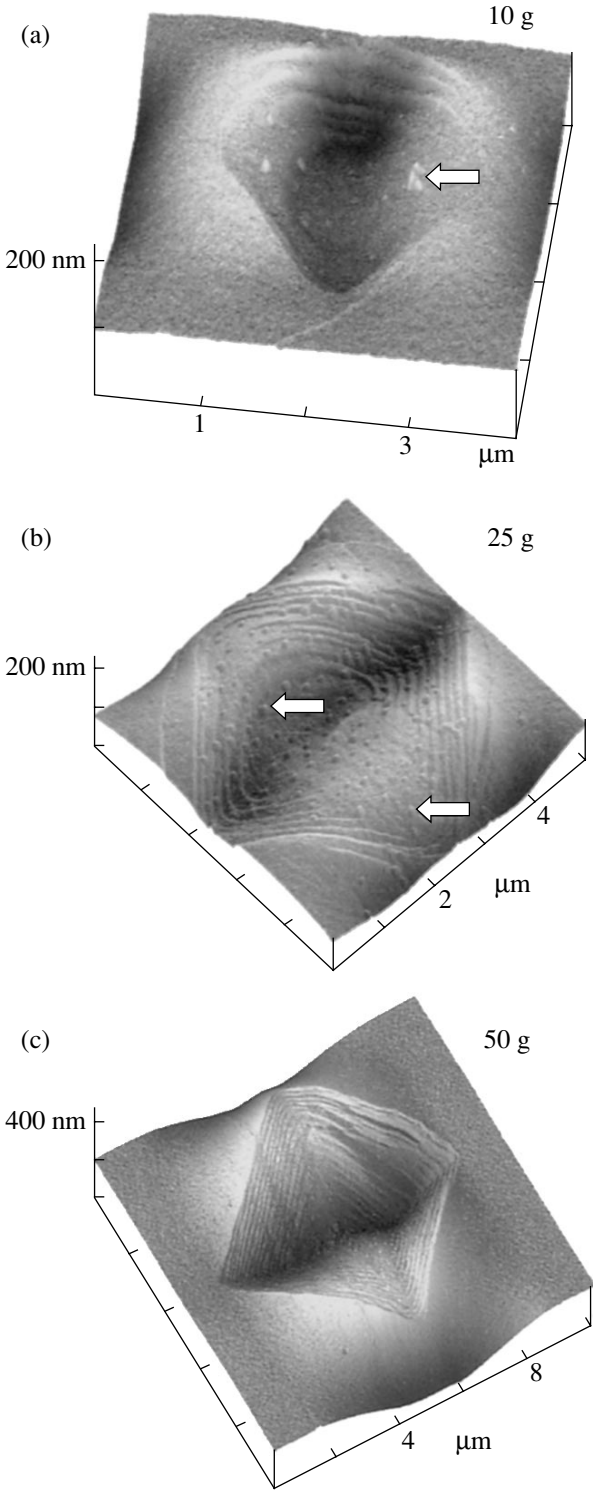

Fig. 6. AFM images of regions with localized deformation in a Ti–Cr–B–N film indented with a Vickers pyramid at a load of (a) 10, (b) 25, and (c) 50 g. Particles rejected outside are shown by arrows.

along the faces of the indenter pyramid. Table 4 gives the critical applied loads for the formation of shear bands. The topography of the Ti–Cr–B–N film surface

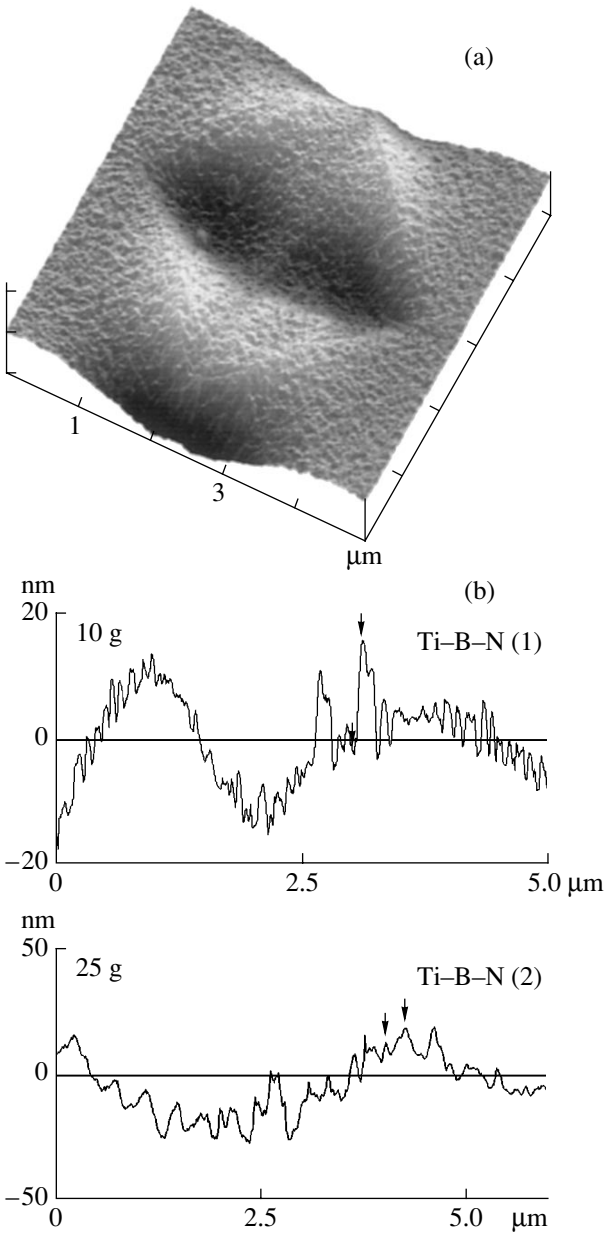

Fig. 7. (a) AFM image and (b) line scans of regions with localized deformation in Ti–B–N films indented with a Vickers pyramid at a load of (a) 50 and (b) 10 and 25 g.

in the regions of localized deformation at loads of 10, 25, and 50 g is shown in Fig. 6. The height and width of the plastic-strain steps are 5–15 and 100–200 nm, respectively (irrespective of the applied load). As the load increases, the number of steps increases but the spacing between them remains unchanged.

Figure 7a shows an image of an indentation made with the Vickers pyramid at a load of 50 g in the Ti–B–N (2) film; the image was taken with an atomic-force scanning microscope. In the Ti–B–N system, no shear bands or radial cracks were observed over the whole range of applied loads, which indicates the homoge-

neous character of the film deformation. From line scans taken from vertical sections of indentations (Fig. 7b), it follows that the film surface relief in a deformed region and the roughness of the initial film surface have virtually the same scale. This is evidence that localized deformation develops via slipping of CSEs along the direction of an applied load. This conclusion is illustrated by an AFM image of an indentation made with the Vickers pyramid (Fig. 8). The cooperative motion of columnar grains along the applied load is seen to occur, with the width of each step being 1–3 columns. The shape of the ends of columns remains unchanged during deformation, and the film surface topography in the indentation is identical to that of the film surface.

The appearance of ejected particles on the terraces of steps is noteworthy. This phenomenon was also observed in [12], but no explanation was provided for it. The size of the particles (100–200 nm) agrees well with the size of individual islands on the surface of the initial films observed in topographic examination. It follows that some CSEs are ejected outside in the course of unloading. Thus, the ejected particles on the terraces of steps are likely to be the apices of individual CSEs (columnar grains or portions of the material).

It was assumed in [9, 11, 12] that homogeneous deformation could occur only in films with a columnar structure. However, the results of this work do not support this assumption. We failed to detect periodic regions of plastic deformation in the form of steps in the fractographs of an indentation made by the Vickers pyramid in Ti–B–N films without a pronounced columnar structure. Analysis of the results (Tables 1, 2) shows that none of the structural parameters or mechanical properties, taken separately, characterizes the deformation mechanism. However, it was found that the quantity H^3/E^2, which characterizes the resistance of the material to plastic deformation [6, 21], allows one to predict the formation of shear bands in the process of localized deformation: steps were formed only at low values of the parameter H^3/E^2. This follows from the theoretical analysis performed by Johnson [22], where it was shown that the load P required for the beginning of plastic deformation in the case where an undeformable ball of radius r is indented into a semi-infinite solid is given by the expression $P = 0.78r^2(H^3/E^2)$. Note that the plastic component in the case of inhomogeneously deformed coatings is larger than in the case of the Ti–B–N coatings deformed without step bands (see parameter W_e in Table 2). Thus, a comparison of the film surface topography before deformation and the film surface relief in the region of an indentation made by a Vickers pyramid, on the one hand, with the size of particles ejected after unloading, on the other, shows that both deformation mechanisms proceed through slipping of CSEs (separate grains or multigrain portions of the material) along the applied load. The results obtained indicate that grain-boundary slip is the main mechanism of deformation in both cases. In the case of inhomogeneous deformation, cooperative motion of the CSEs takes place because of the larger binding energy between columns. Deformation proceeds at a constant volume and is accompanied by the rejection of an amount of deformed material outside (the formation of hillocks) and/or by elastic compression. Upon unloading, individual CSEs can be rejected outside due to the elastic-stress relaxation or the reverse plasticity, which causes the appearance of ejected particles (visible in Figs. 6, 7a).

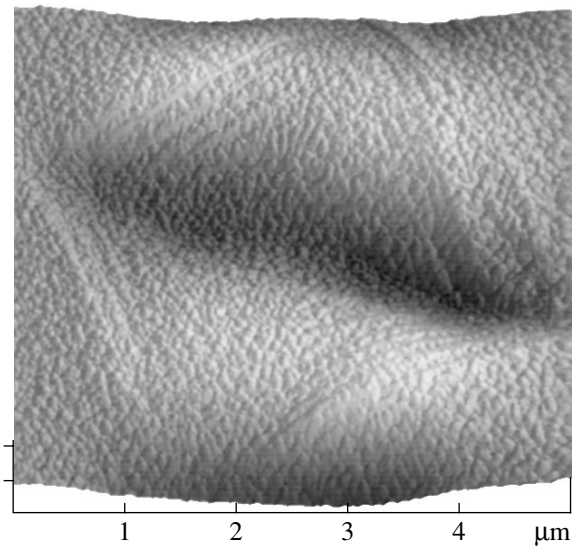

Fig. 8. Fractograph of the fracture surface of a Ti–Si–N film indented with a Vickers pyramid at a load of 25 g.

4. PHYSICAL-MECHANICAL PROPERTIES

The values of the hardness, modulus of elasticity, and elastic recovery of films are given in Table 2. The depth of indentation for all loads was smaller than 15% of the film thicknesses. The Ti–B–N (2) film had the maximum hardness (42 GPa). Young's modulus for coatings of this system varied in the range 250–300 GPa, which is significantly lower than that for bulk TiN and TiB_2 compounds [23]. The Ti–B–N films also had the maximum value of elastic recovery (77–81%) and the minimum plastic deformation (23–19%). Note that shear bands formed only in the films with large plastic deformation.

An important advantage of multicomponent nanostructured films is that one can fabricate superhard materials with identical hardness and different values of the Young's modulus (Table 5). This means that thin films with identical hardness can differ in their elastic strain to failure (H/E) and the resistance to plastic deformation (H^3/E^2). Their elastic properties can also be significantly different. A combination of high hardness and elastic recovery characterizes multicomponent nanostructured films as new unique hard and, at the same time, elastic materials. It is also important that

different materials can have virtually the same mechanical properties (e.g., Ti–Zr–C–O and Ti–B–N films, see Table 5). Thus, superhard coatings can be produced with different combinations of elastic and plastic properties, which provides a wide choice of coatings for various specific tasks.

Additional studies should be made to determine the E and W_e values required for high wear resistance of a material. One of the indubitable advantages of films with a low modulus of elasticity is that such films better fit steel substrates (E = 205 GPa), which minimizes the elastic stresses at the coating/substrate interface and the internal residual stresses in the system, thereby significantly decreasing the wear [6].

5. CONCLUSIONS

Thus, we have found that multicomponent nanostructured films deposited through magnetron sputtering have either a pronounced or a latent columnar structure; such a structure plays a significant role and manifests itself in deformation. Localized deformation in nanostructured thin films can develop both homogeneously and inhomogeneously (with the formation of shear bands). To predict the formation of shear bands in a material subjected to deformation, we can use the parameter H^3/E^2, which describes the resistance of the material to plastic deformation. Both deformation mechanisms involve slipping of CSEs (individual grains or multigrain portions of the material) along the direction of the applied load. In the case of a weak chemical bond between neighboring grains, individual CSEs can be rejected outside as a result of relaxation of elastic stresses upon unloading. The inhomogeneous deformation mechanism is associated with cooperative motion of CSEs due to the large binding energy between grains.

ACKNOWLEDGMENTS

This work was supported by the International Science and Technology Center (ISTC), grant no. 1852.

REFERENCES

1. D. V. Shtansky, K. Kaneko, Y. Ikuhara, and E. A. Levashov, Surf. Coat. Technol. **148** (2–3), 204 (2001).
2. D. V. Shtanskiĭ and E. A. Levashov, Izv. Vyssh. Uchebn. Zaved., Tsvetn. Metall. **3**, 52 (2001).
3. D. V. Shtansky, E. A. Levashov, A. N. Sheveiko, and J. J. Moore, J. Mater. Synth. Process. **7** (3), 187 (1999).
4. D. V. Shtansky, E. A. Levashov, A. N. Sheveiko, and J. J. Moore, J. Mater. Synth. Process. **6** (1), 61 (1998).
5. A. Niederhofer, P. Nesládek, H.-D. Männling, *et al.*, Surf. Coat. Technol. **120–121**, 173 (1999).
6. A. Leyland and A. Matthews, Wear **246** (1–2), 1 (2000).
7. S. Vepřek, J. Vac. Sci. Technol. A **17** (5), 2401 (1999).
8. J. Musil, Surf. Coat. Technol. **125** (1–3), 322 (2000).
9. R. A. Andrievskiĭ, G. V. Kalinnikov, and D. V. Shtanskiĭ, Fiz. Tverd. Tela (St. Petersburg) **42** (4), 741 (2000) [Phys. Solid State **42**, 760 (2000)].
10. S. Vepřek and S. Reiprich, Thin Solid Films **268** (1–2), 64 (1995).
11. R. A. Andrievski, G. V. Kalinnikov, and D. V. Shtansky, Mater. Res. Soc. Symp. Proc. **581**, 583 (2000).
12. R. A. Andrievski, G. V. Kalinnikov, J. Jauberteau, and J. Bates, J. Mater. Sci. **35** (11), 2799 (2000).
13. R. A. Andrievsky and G. V. Kalinnikov, Surf. Coat. Technol. **142–144**, 573 (2001).
14. D. V. Shtansky, S. A. Kulinich, E. A. Levashov, *et al.*, Thin Solid Films **420–421**, 330 (2002).
15. V. A. Movchan and A. V. Demchishin, Fiz. Met. Metalloved. **83**, 83 (1969).
16. J. A. Thornton, J. Vac. Sci. Technol. **11** (4), 666 (1974).
17. E. A. Levashov, A. S. Rogachev, V. I. Yukhvid, and I. P. Borovinskaya, *Physicochemical and Technological Fundamentals of Self-Propagating High-Temperature Synthesis* (BINOM, Moscow, 1999).
18. W. C. Oliver and G. M. Pharr, J. Mater. Res. **7** (6), 1564 (1992).
19. H. Ljungcrantz, C. Engstrom, L. Hultman, *et al.*, J. Vac. Sci. Technol. A **16** (5), 3104 (1998).
20. V. I. Trofimov and V. A. Osadchenko, Sov. J. Technol. **60** (8), 540 (1993).
21. T. Y. Tsui, G. M. Pharr, W. C. Oliver, *et al.*, Mater. Res. Soc. Symp. Proc. **383**, 447 (1995).
22. K. L. Johnson, *Contact Mechanics*, 1st ed. (Cambridge Univ. Press, Cambridge, 1985), p. 155.
23. R. A. Andrievskiĭ, G. V. Kalinnikov, N. P. Kobelev, *et al.*, Fiz. Tverd. Tela (St. Petersburg) **39** (10), 1859 (1997) [Phys. Solid State **39**, 1661 (1997)].
24. J. Musil and H. Hrubý, Thin Solid Films **365** (1), 104 (2000).
25. J. Musil, F. Kunc, H. Zeman, and H. Poláková, Surf. Coat. Technol. **154** (2–3), 304 (2002).

Translated by K. Shakhlevich